Actin Structure and Function: Roles in Mitochondrial Organization and Morphogenesis in Budding Yeast and Identification of the Phalloidin-binding Site

David G. Drubin, Heather D. Jones, and Kenneth F. Wertman*

Department of Molecular and Cell Biology, University of California, Berkeley, California 94720

To further elucidate the functions of actin in budding yeast and to relate actin structure to specific roles and interactions in vivo, we determined the phenotypes caused by 13 charged-to-alanine mutations isolated previously in the single *Saccharomyces cerevisiae* actin gene. Defects in actin organization, morphogenesis, budding pattern, chitin deposition, septation, nuclear segregation, and mitochondrial organization were observed. In wild-type cells, mitochondria were found to be aligned along actin cables. Many of the amino acid substitutions that had the most severe effects on mitochondrial organization are located under the myosin "footprint" on the actin monomer, suggesting that actin-myosin interactions might underlie mitochondrial organization in yeast. In addition, one mutant (*act1-129*; R177A, D179A) produced an actin that assembled into cables and patches that could be visualized by anti-actin immunofluorescence in situ and that assembled into microfilaments of normal appearance in vitro as judged by electron microscopy but which could not be labeled by rhodamine-phalloidin in situ or in vitro. Rhodamine-phalloidin could label actin filaments assembled from all of the other mutant actins, including one (*act1-119*; R116A, E117A, K118A) that is altered at a residue (E117) that can be chemically cross-linked to phalloidin. The implication of residues R177 and/or D179 in phalloidin binding is in close agreement with a recently reported molecular model in which the phalloidin-binding site is proposed to be at the junction of two or three actin monomers in the filament.

INTRODUCTION

The budding yeast *Saccharomyces cerevisiae* expresses a single actin encoded by the *ACT1* gene (Gallwitz and Seidel, 1980; Ng and Abelson, 1980). Roles for yeast actin have been suggested by studies on actin organization (Adams and Pringle, 1984; Kilmartin and Adams, 1984) and also were demonstrated by phenotypic studies (Novick and Botstein, 1985) on two mutant alleles of *ACT1* that were created by random mutagenesis (Shortle *et al.*, 1984). Recently, the development of atomic models for monomeric and polymeric rabbit muscle actin has provided an opportunity to understand the mechanism of actin-based processes in terms of molecular interactions in three-dimensional (3-D) space (Holmes *et al.*, 1990; Kabsch *et al.*, 1990; Lorenz *et al.*, 1993). Significantly, because yeast and rabbit actin are very similar in primary structure (88% amino acid identity) (Gallwitz and Seidel, 1980; Ng and Abelson, 1980)

and in biochemical properties (Greer and Schekman, 1982; Kron *et al.*, 1992; Nefsky and Bretscher, 1992), the atomic structural model of rabbit actin is likely to reflect closely the structure of yeast actin. Thus, the phenotypic effects of mutations in yeast actin can now be interpreted in the context of their effects on spatially defined regions of the protein.

The two original *act1* mutations (Shortle *et al.*, 1984) lie near each other in one of actin's four subdomains (subdomain 2) (Kabsch *et al.*, 1990) and an additional mutation isolated subsequently (Dunn and Shortle, 1990) lies in subdomain 4. More recently, complementary strategies were used to make site-directed mutations in many additional regions of yeast actin. One strategy (Johannes and Gallwitz, 1991; Cook *et al.*, 1992, 1993) involved altering residues previously implicated in specific aspects of actin function and provided powerful tests of the roles of these residues. The aim of the other strategy (Wertman *et al.*, 1992), called scanning charged-to-alanine mutagenesis (Bass *et al.*, 1991; Bennett *et al.*, 1991; Gibbs and Zoller, 1991), was to target for sub-

---

stitution those residues exposed on the actin surface without regard to whether the residues had been implicated in any particular interaction. Residues situated on the surface of actin are likely to be important for protein-protein and protein-ligand interactions and are less likely to be important for protein folding and stability. The majority of the 36 charged-to-alanine mutations in yeast actin are exposed on the surface of the monomer (Wertman *et al.*, 1992; Wertman and Drubin, 1992).

For the first level of analysis of the effects of the charged-to-alanine actin mutations, tests of the sensitivity of growth of mutant strains to different temperatures and to osmotic stress and genetic tests for dominance have revealed that the mutations have diverse effects on actin function (Wertman *et al.*, 1992). The second level of analysis, presented here, aims to elucidate the importance of different regions of actin for various cellular processes and molecular interactions. We present here a phenotypic analysis of 13 conditional-lethal yeast charged-to-alanine actin mutations. These mutations reside in many different regions of the surface of actin (Wertman *et al.*, 1992; Wertman and Drubin, 1992). The results increase our knowledge of the biological roles of actin in yeast. Defects in morphogenesis, budding pattern, actin organization, nuclear segregation, mitochondrial organization, and, in one case, phalloidin binding, were observed.

MATERIALS AND METHODS

Strains, Media, and Culture Conditions

The yeast strains used in this study are listed in Table 1. For all experiments cells were grown in YEPD medium (1% yeast extract, 2% bacto peptone, and 2% glucose) in rotary shaking water baths.

Microscopic Analysis of Yeast Cells

Immunofluorescent localization of actin was as described by Drubin *et al.* (1988). The cells were mounted in mounting medium containing the DNA staining dye 4′,6-diamidino-2-phenylindole dihydrochloride (DAPI) as described by Pringle *et al.* (1989). For Nomarsky optics, cells were fixed by adding formaldehyde directly to cultures of growing yeast cells to a final concentration of 3.7%. After a brief sonication to dissociate aggregated cells, the cells were viewed and photographed using a Zeiss Axioskop microscope (Thornwood, NY). Hypersensitized Technical Pan film (Kodak, Rochester, NY) (Schulze and Kirschner, 1986) was used for all photography. Preparation of affinity-purified anti-yeast actin antisera was described by Drubin *et al.* (1988). All fluorescent secondary antisera were obtained from Organon Teknika-Cappel (Malvern, PA).

Analysis of Bud Scar Patterns

Bud patterns were determined by staining cells with the chitin-specific dye calcofluor as described by Pringle *et al.* (1989). Microscopic observations were made on log phase diploid cells bearing at least three bud scars. At least 100 cells of each genotype were scored as described in the legend to Table 3.

In Vitro Actin Assembly and Visualization

Yeast actin was purified by DNase I affinity chromatography as described by Kron *et al.* (1992). The actin (1.0 μM final concentration)

in G buffer (5 mM tris(hydroxymethyl)aminomethane [Tris] 7.4, 0.2 mM ATP, 0.2 mM dithiothreitol [DTT], 0.05 mM $MgCl_2$) was assembled into filaments by adding 0.1 volume of 10× assembly initiator buffer (0.1 M Tris 7.4, 50 mM $MgCl_2$, 5.0 mM ATP) and allowing the solution to incubate at room temperature for 60 min. Rhodamine phalloidin (Molecular Probes, Eugene, OR) was then added to each assembly reaction to a final concentration of 2 μM. The filaments were visualized by adding 1 μl of the above solution to 50 μl of 1× assembly initiator buffer supplemented with 100 mM DTT as an anti-bleaching agent (Kron *et al.*, 1992), and a few microliters of this solution was placed under a glass coverslip on a microscope slide. The rhodamine-phalloidin-labeled actin filaments were visualized using a Zeiss Axioskop fluorescence microscope with a HB100 W/Z high pressure mercury lamp and a Zeiss 100× Plan-Neofluar oil immersion objective, or, for recording the images shown in Figure 7, c and d, the samples were viewed on a Nikon inverted microscope (Garden City, NY) and imaged with a 1320 × 1024 pixel CCD chip (Kodak) in a cooled camera (Photometrics, Tucson, AZ). Images were processed (Perceptics software) on a Mac IIx computer (Apple Computers, Cupertino, CA) and stored on the hard disc. Photographs of the images were made directly off of the computer monitor using Kodak Technical Pan film. Another aliquot from each assembly reaction was removed and negatively stained as described by Millonig *et al.* (1988) except that 1% aqueous uranyl acetate was used.

RESULTS

Cell Morphology and Budding Pattern

Previous studies showed that actin function is important for yeast morphogenesis (Novick and Botstein, 1985; Read *et al.*, 1992). To determine whether the charged-to-alanine actin mutations cause defects in morphogenesis, 13 isogenic diploid strains homozygous for different conditional-lethal *act1* alleles (Table 1) were grown in log phase cultures at the permissive temperature (25°C), shifted for 90 min to the nonpermissive temperature (37°C), and examined using Nomarsky optics. An actin hemizygote (*ACT1/act1-Δ1 :: LEU2*) was also analyzed. A number of different morphological phenotypes were observed and tabulated (Figure 1 and Table 2). Micrographs of representative cells having each phenotype are shown in the figures, and the variety of phenotypes displayed by the 15 different isogenic strains (13 point mutants, an *ACT1/act1-Δ1 :: LEU2* hemizygote, and a wild type strain) are summarized in the tables. Figure 1, panel 1 shows three fields of wild-type diploid cells. These cells are of fairly uniform size. They are ellipsoid in shape, and a single bud is often found at one end of the cell. Panel 2 of Figure 1 shows cells that have a septation defect leading to a multibudded phenotype. A similar defect is seen in panel 3 of Figure 1 that shows cells with two buds. Panel 4 of Figure 1 shows that some actin mutants (e.g., *act1-119*, *act1-120*) appear to have wide bud necks compared to wild-type cells (panel 1). Panel 5 of this figure shows *act1-124* cells with the "bumpy cell" phenotype (arrowheads). These bumps often create the impression that the cells are square or rectangular. In panel 6 of Figure 1, cells with the "elongated bud" phenotype are shown. These elongated buds are often several times longer than a wild-type cell and are quite variable in both appearance and length. Another morphological phenotype is the appearance of

Table 1. Strains used in this study

Strain[a]	Genotype (partial)[b]
DDY430	act1-119::HIS3/act1-119::HIS3
DDY431	act1-129::HIS3/act1-129::HIS3 can1-1/+
DDY432	act1-111::HIS3/act1-111::HIS3 can1-1/+
DDY433	act1-120::HIS3/act1-120::HIS3 can1-1/can1-1
DDY434	act1-124::HIS3/act1-124::HIS3 can1-1/+
DDY435	act1-125::HIS3/act1-125::HIS3 can1-1/can1-1
DDY436	act1-132::HIS3/act1-132::HIS3 can1-1/can1-1
DDY437	act1-133::HIS3/act1-133::HIS3
DDY438	act1-108::HIS3/act1-108::HIS3 can1-1/+
DDY439	act1-101::HIS3/act1-101::HIS3
DDY440	ACT1::HIS3/ACT1::HIS3 can1-1/can1-1
DDY441	act1-113::HIS3/act1-113::HIS3 can1-1/can1-1
DDY442	act1-121::HIS3/act1-121::HIS3 can1-1/can1-1
DDY443	act1-136::HIS3/act1-136::HIS3
DDY444	act1-Δ1::LEU2/+ can-1/+ cry1/+

[a] All strains used in this study are diploids made for this study by crossing pairs of a and α strains containing the same alanine scan act1 allele (Wertman et al., 1992).

[b] All strains are a/α ura3-52/ura3-52 leu2-3,112/leu2-3,112 his3Δ200/his3Δ200 tub2-201/tub2-201 ade4/+ ade2/+, except DDY444, which is tub2-201/+ at the TUB2 locus. Only alleles that vary between strains are shown above.

abnormally small cells as shown in panel 7 of Figure 1 (arrowheads). Finally, the large cell phenotype (Figure 1, panel 8) was seen for many strains and was particularly prominent for act1-108 and act1-133 cells. The enlarged cells often have large vacuoles.

One of the steps in the organization of a bud site early in the cell cycle is the assembly of a ring of cortical actin structures, each of which presumably contains filamentous actin because they can be stained by fluorochrome-conjugated phalloidin (Adams and Pringle, 1984). This ring is concentric with a ring of 10-nm neck filaments and a ring of intense chitin staining (see Ford and Pringle, 1991 and the references therein). The chitin ring remains after septation, marking the point of bud formation with a "bud scar". Budding occurs with a stereotypical pattern that differs between a or α haploid cells (axial budding) and a/α diploid cells (bipolar pattern) (see Drubin, 1991 for a description of budding patterns). To determine whether any of the charged-to-alanine actin mutations cause defects in the bud site selection pattern, the bud scars of diploid cells grown in log phase cultures at 25°C were stained with calcofluor. The budding patterns for each strain are tabulated in Table 3. As expected for a wild-type diploid strain, the majority of the ACT1/ACT1 cells (73%) were scored as bipolar. In addition, a smaller but significant population (24%) was scored as having an axial budding pattern, and only 3% were scored as having a random budding pattern. A strain that is hemizygous for the ACT1 gene (DDY444) showed a significant decrease in both the bipolar (34%) and axial (3%) budding patterns with 63% of the cells showing a random budding pat-

tern. Each of the charged-to-alanine act1 mutations also caused a decrease in the proportion of cells with bipolar and axial budding patterns and an increase in cells with random budding patterns (Table 3). In addition, seven of the 12 charged-to-alanine mutants examined, but not the ACT1/act1-Δ1::LEU2 hemizygote, showed defects in chitin deposition that are manifested as increased uniform chitin staining and/or staining in patches rather than, or in addition to, circular bud scars (Table 3). For four strains, the high background of calcofluor staining precluded the scoring of budding patterns (Table 3).

Actin Organization

Anti-actin immunofluorescence was used to determine how actin is organized in the charged-to-alanine actin mutants grown at 25 and 37°C (Figure 2 and Table 4). In wild-type cells, (Figure 1a) a network of cytoplasmic cables course through the cytoplasm. These cables tend to be aligned along the mother-bud axis (Adams and Pringle, 1984; Kilmartin and Adams, 1984). At regions of the cell cortex that are either actively growing or are about to grow, brightly staining cortical patches of actin are present (Adams and Pringle, 1984). A number of defects in actin organization were observed in the actin mutants and the ACT1/act1-Δ1::LEU2 hemizygote. Intensely staining actin bars are present in several mutant alleles (Figure 2, b and c), and these bars often appear closely associated with the nucleus (Table 4). A phenotype observed for a number of mutant alleles and for the hemizygote at 37°C (Table 4) is delocalization of the cortical actin patches (Figure 2, d and e). The delocalized cortical patch phenotype often coincides with an absence or near absence of actin cables (Figure 2, d and e) and is prominent for those mutants that tend to be enlarged and multinucleate (see below). Several act1 mutant alleles cause the formation of cortical actin patches that, compared to the patches in wild-type cells, are fewer in number but are larger and chunklike in appearance (Figure 2, f-h). These structures are reminiscent of the actin structures seen in sla1 mutants grown at 25°C (Holtzman et al., 1993). Some act1 mutants have high diffuse backgrounds of actin staining (Figure 2, g and h), suggesting that they might have elevated pools of unassembled actin, and others (Figure 2i) have both diffuse background staining and abnormally small cortical actin patches.

Nuclear Segregation

For several reasons, we thought that the charged-to-alanine actin mutants might show abnormalities in nuclear number. First, yeast actin mutants are defective in morphogenesis, and morphogenetic mutants often have defects in nuclear segregation (Adams et al., 1990; Bender and Pringle, 1991). Second, actin function was recently shown to be important for ori-
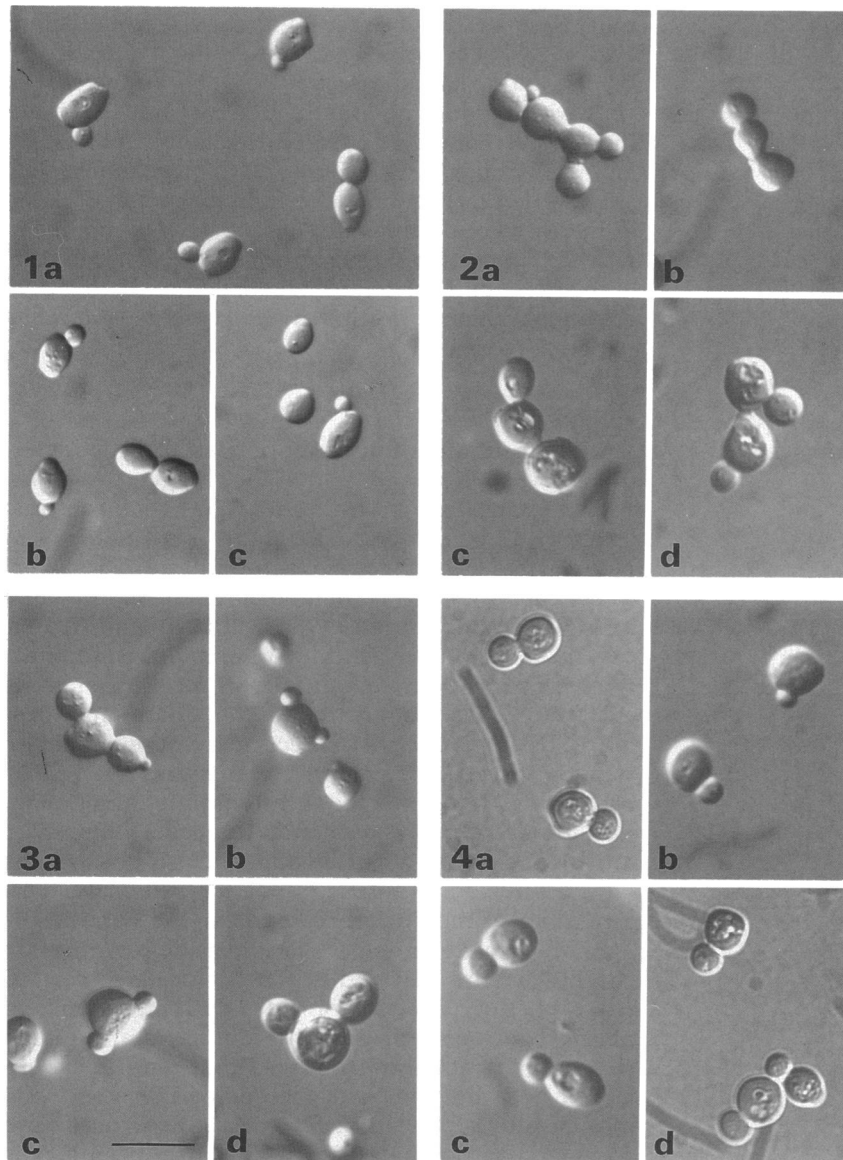
Figure 1. Nomarsky optics showing morphologies of sonicated diploid wild-type and actin mutant cells. 1, a–c, wild-type, 25°C; 2, a and b, *act1-124/act1-124*; 25°C; 2c, *act1-133/act1-133*, 25°C; 2d, *act1-133/act1-133*, 37°C, 90 min; 3a, *act1-121/act1-121*, 25°C; 3b, *act1-124/act1-124*, 25°C; 3c, *act1-111/act1-111*, 25°C; 3d, *act1-133/ act1-133*, 25°C; 4a, *act1-120/act1-120*, 25°C; 4b, *act1-119/act1-119*, 37°C, 90 min; 4c, *act1-119/ act1-119*, 37°C, 90 min; 4d, *act1-119/act1-119*, 25°C; 5, a–c, *act1-124/act1-124*, 25°C; 6, a–c, *act1-121/act1-121*, 25°C; 7, a and c, *act1-120/ act1-120*, 37°C, 90 min; 7b, *act1-120/act1-120*, 25°C; 8a, *act1-133/act1-133*, 25°C; 8, b and c, *act1-108/act1-108*, 25°C. Arrowheads in panel 5 indicate bumpy cells, and in panel 7 indicate small cells. Bar, 10 μm.

entation of the mitotic spindle in yeast (Palmer *et al.*, 1992) and is important for nuclear migration into mating projections (Read et al., 1992). Third, *tpm1* (tropomyosin) and *myo2* (myosin) mutants are multinucleate (Johnston *et al.*, 1991; Liu and Bretscher, 1992). We examined the disposition of nuclei in the *act1* mutants by staining with the DNA dye DAPI. Figure 3, a and b show actin immunofluorescence and DAPI staining, respectively, for the same field of wild-type diploid cells. The DAPI staining shows that each cell has a single nucleus (the weakly staining material organized in string-like structures is mitochondrial DNA, see below). Most of the *act1* mutants and the *ACT1/act1-Δ1::LEU2* hemizygote have an increased tendency to accumulate abnormal numbers of nuclei (see Table 4). Figure 3 shows a cell with delocalized cortical actin patches and six nuclei (c and d), and

a large budded cell in which the mother cell and bud each have three nuclei (e and f). In some cases, events were observed that appear to be leading to the formation of multinucleate cells. In Figure 3, h and j mitotic division is occurring completely within two mother cells, rather than through the mother-daughter bud necks. In one case (Figure 3j), nuclear division is occurring in a multinucleate cell. One nucleus appears to be oriented correctly in the mother-daughter neck, whereas the other is dividing within the mother.

Mitochondrial Organization in Actin Mutants

In wild-type yeast cells, mitochondria, as visualized by DAPI staining, appear as string-like structures. Figure 4, b, d, and f, which are intentionally overexposed, show
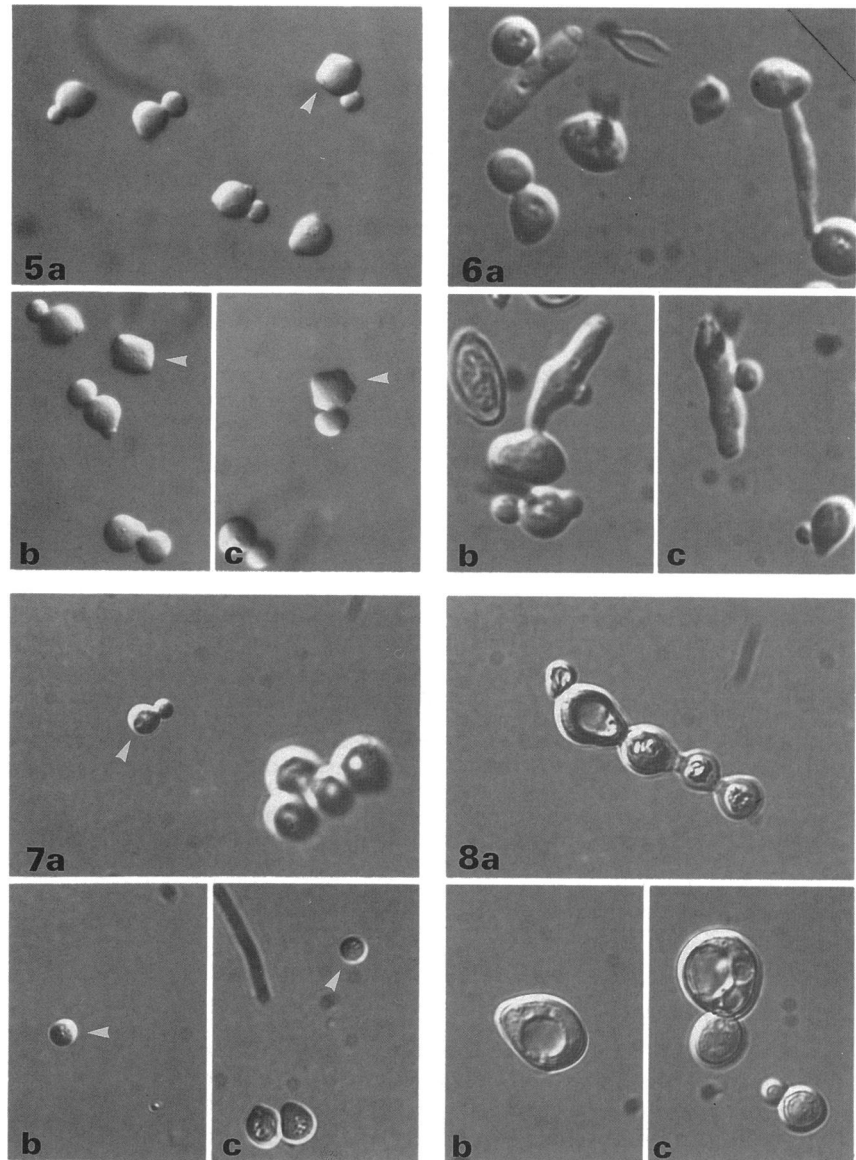
Figure 1. (Continued)

the organization of mitochondria in wild-type diploid cells. In certain *act1* mutants (Table 4), the mitochondrial genomes appear condensed and/or clumped (Figure 4, h, j, l, n, and p). In some cases (Figure 4, k–n) the mutant cells with defective mitochondrial organization contained no detectable actin cables. In other cases (Figure 4, g–j, o, and p), the mutant cells contained fairly elaborate networks of cytoplasmic actin cables.

Mitochondrial Association with Actin Cables in Wild-type Cells

Because actin mutants had aberrantly organized mitochondria, the organization of actin cables and mitochondria in wild-type yeast cells were compared by fluorescence microscopy. Shown in Figure 5 is anti-actin immunofluorescence (column 1) and DAPI

staining (column 2) of the same fields of cells. The DAPI staining is intentionally overexposed for better visualization of mitochondrial DNA. The third column shows traces of the images in the first two columns. The stippled structures represent actin, and the black structures represent mitochondria. Mitochondrial strings often coalign with actin cables over long stretches, although not every actin cable has mitochondria associated with it. The colocalization of mitochondrial strings with actin cables was clearly evident in about 20% of all wild-type cells examined. This may be an underestimate of the extent of mitochondrial association with actin cables. The small size of yeast cells and the fact that there are often many actin cables in the cytoplasm can preclude the identification of favorable focal planes for observing colocalization of actin cables and mitochondria.

Table 2. Morphogenic defects of actin mutants

ACT1 Allele	Bumps (+/−)		Two buds (%)		Multibuds (%)		Large cells (%)		Small cells (%)		Wide necks (+/−)		Long buds (%)	
	25°C	37°C	25°C	37°C	25°C	37°C	25°C	37°C	25°C	37°C	25°C	37°C	25°C	37°C
WT/WT	−	−	−	−	−	−	−	−	−	−	−	−	−	−
WT/Δ	−	+	−	2.9	−	0.5	−	−	−	−	−	−	−	−
101/101	+	−	−	−	−	−	−	−	−	−	−	−	−	−
108/108	+	−	1.7	3.2	−	−	15.7	10.4	0.8	7.6	−	−	−	−
111/111	−	−	3.5	13.7	−	−	−	−	5.1	−	−	−	−	−
113/113	+	++	ND	12.6	−	3.5	−	−	−	−	−	−	−	−
119/119	+	+	−	7.5	3.2	6.0	0.9	−	−	−	+	ND	−	−
120/120	−	−	4.1	0.4	−	−	2.3	−	3.2	4.1	+	+	−	−
121/121	+	−	3.1	4.9	2.7	6.4	−	−	−	−	−	−	14.7	6.9
124/124	+	+	2.2	8.3	1.4	2.9	−	−	−	−	−	−	−	−
125/125	−	−	4.2	2.1	−	−	−	−	10.8	4.5	−	−	−	−
129/129	−	+	−	1.5	−	−	−	−	−	−	−	−	−	−
132/132	−	−	−	−	−	−	−	−	−	−	+	ND	−	−
133/133	−	−	1.3	8.1	14.7	5.7	8.2	11.0	−	−	+	ND	−	−
136/136	ND	−	ND	7.5	ND	2.0	ND	−	ND	−	ND	−	ND	−

Log phase cultures of cells were grown at 25°C and were shifted to 37°C for 90 min. At least 200 formaldehyde-fixed cells (3.7% formaldehyde) were counted under Nomarsky optics for each condition and phenotype. Phenotypes were scored as + or − for bumps and wide necks or as a % of total cells that show the phenotype for all other phenotypes. A "−" in columns for phenotypes other than bumps and wide necks indicates that no cells with that phenotype were observed.

ND: not determined; *bumps:* distinct bumps protrude from the otherwise smooth surface of the cell (Figure 1, panel 5, arrowheads); *two buds:* one cell with two buds, not necessarily of the same size, attached to it (Figure 1, panel 3). The buds often were at an angle to each other that created a "Mickey Mouse"-like image; *multibuds:* similar to the two bud cells, except that three or more unseparated cells were arrayed in a line, often creating a snowman-like image (Figure 1, panel 2); *large cells:* cells were about 3–4 times larger in diameter than wild-type cells. Many of the mutants had enlarged cells in their populations but only those alleles that showed exceptional enlargement as defined above were scored for this phenotype; *small cells:* cells had about 1/2 the diameter of wild-type cells (Figure 1, panel 7, arrowheads); *wide necks:* cells appeared to have significantly larger necks than wild-type cells (Figure 1, panel 4). This phenotype might be a consequence of increased roundness of the cells, or it might be a consequence of the bud necks being larger. A strain was scored as "+" if >10% of the population had the phenotype; *long buds:* buds that are ≥1 1/2 times greater in length than in width. The cells shown in Figure 1, panel 6 are dramatic examples of this phenotype.

Phalloidin Binding

Phalloidin is a cyclic peptide that binds very tightly to actin filaments and stabilizes the filaments against depolymerization (Wieland, 1977). Identification of the phalloidin binding site on the actin filament is of interest because this site is potentially important for biological regulation of actin filament stability. To test the possibility that a charged-to-alanine actin mutation might have affected phalloidin binding, the actin cytoskeleton of each of the conditional-lethal actin mutants listed in Table 1 was probed with both rhodamine-labeled phalloidin and a polyclonal antibody against actin (Figure 6). One mutant allele (*act1-129*) contains actin cables and cortical actin patches that can be visualized with an anti-actin antibody (Figure 6c) but not with fluorochrome-conjugated phalloidin (Figure 6d). Figure 6e shows DAPI staining of the same field photographed for Figure 6d. All other alleles, including those that cause more severe defects in actin organization than the *act1-129* allele, contained cytoplasmic cables and/or cortical actin patches that could be stained with rhodamine-phalloidin. This includes one allele (*act1-119*; R116A, E117A, K118A) for which a residue (E117) that could

be chemically cross-linked to phalloidin (using rabbit muscle actin) (Vandekerckhove *et al.*, 1985) was replaced by alanine (Figure 6, a and b; see also, DISCUSSION).

To verify that the lack of phalloidin staining of the *act1-129* mutant cells is because of an alanine substitution and not because of an indirect effect such as inaccessibility of phalloidin to the actin filaments in the mutant cell, we purified *act1-129* mutant actin, assembled it into filaments, and incubated these filaments in rhodamine phalloidin. Figure 7, a and b shows by electron microscopy that both wild-type and mutant actins form filaments of normal appearance. When these two preparations are stained with rhodamine-phalloidin, the wild-type filaments (Figure 7c), but not *act1-129* mutant filaments (Figure 7d), are labeled.

DISCUSSION

Phenotypes of Charged-to-Alanine act1 Mutants Reveal Actin Functions

Studies on the first two *act1* alleles isolated revealed roles for actin in localized deposition of chitin on the

Table 3. Budding patterns in diploid wild-type and actin mutant cells

		Bud scar pattern (%)[a]		Irregular staining[b]	
ACT1 Allele	Axial	Bipolar	Random	Delocalized	Patches
WT/WT	24	73	3	−	−
WT/Δ	3	34	63	−	−
101/101	9	45	45	−	−
108/108	11	9	80	+	++
111/111	ND	ND	ND	+	+
113/113	3	26	70	+	−
119/119	9	56	35	−	−
120/120	8	56	37	−	−
121/121	ND	ND	ND	++	++
124/124	3	19	78	−	−
125/125	ND	ND	ND	++	++
129/129	7	32	61	−	+
133/133	12	37	51	++	+
136/136	ND	ND	ND	++	++

Bud patterns were determined by staining cells with the chitin-specific dye calcofluor as described in MATERIALS AND METHODS and below.

[a] Percentages were determined by microscopic observation of log phase diploid cells bearing three or more bud scars. Numbers are derived from the analysis of ≥100 cells. Cells were scored as *axial* if the scars were clustered at one end or arranged in a line, *bipolar* if bud scars clustered at both ends of the cell, and *random* if the scars were dispersed on the surface of the cell rather than clustered at one or both ends (Chant and Herskowitz, 1991). ND, not determined because background staining was too high to allow determination of bud scar patterns.

[b] Some cells had irregular calcofluor staining of chitin. *Delocalized:* a generalized diffuse (often intense) cell wall staining; *patches:* amorphous intense concentrations of cell wall staining were observed.

cell surface, secretion of the periplasmic protein invertase, and cellular morphogenesis (Novick and Botstein, 1985; Read *et al.*, 1992). In addition, actin mutants showed an intracellular accumulation of secretory vesicles, death of cells in the budded portion of the cell cycle upon prolonged incubation at the restrictive condition, and osmotic sensitivity (Novick and Botstein, 1985; see also Chowdhury *et al.*, 1992). Subsequent studies on these two mutants and on one additional mutant allele demonstrated the importance of actin for endocytosis (Kubler and Riezman, 1993), mating projection formation, nuclear migration in response to mating pheromone (Read *et al.*, 1992), and the maintenance of proper spindle orientation (Palmer *et al.*, 1992).

Here we have examined the in vivo consequences of 13 charged-to-alanine *act1* mutations to investigate further the function of actin in budding yeast and to identify the regions of the actin monomer and filament that are responsible for specific functions. Our studies have confirmed many of the conclusions about actin functions drawn from the studies mentioned above and have provided evidence for additional roles of actin. Thus, although these studies have corroborated roles for actin in chitin localization and morphogenesis, we have now established the importance of actin function for bud site selection and spatial organization of mitochondria. The severity of the phenotypic defects observed for the various strains correlated well with the previously reported growth characteristics of the strains. For example,

act1-119, *act1-120*, and *act1-129* strains grown at 25°C had moderate defects in actin and mitochondrial organization (Table 4), and strains carrying these alleles grew well over a broad temperature range (Wertman *et al.*, 1992). On the other hand, *act1-132*, *act1-133*, and *act1-136* strains had more severe phenotypic defects and grew over narrower temperature ranges.

Late in the cell cycle actin (as visualized by phalloidin staining but not by immunofluorescence) (Kilmartin and Adams, 1984) is organized as a single or double bar at the bud neck and subsequently, (as visualized by phalloidin staining or immunofluorescence) as a concentration of patches at the neck (Adams and Pringle, 1984; Kilmartin and Adams, 1984). This spatial pattern is suggestive of a role in septum formation. In support of this possibility, Novick and Botstein (1985) reported an increase in the incidence of two-budded cells in actin mutants. In addition, *myo1* mutants were reported to be defective in cytokinesis (Watts *et al.*, 1987). Because myosin is only known to function in conjunction with actin, this latter finding provides further support for the possibility that actin functions in septum formation. In the present study, we have found that a common phenotype that varies considerably in severity from *act1* allele to allele is the accumulation of two-budded and multibudded cells. Considered together, the above evidence strongly implicates actin in septum formation. Actin appears to function in both cytokinesis and cell wall separation because digestion of the cell walls of
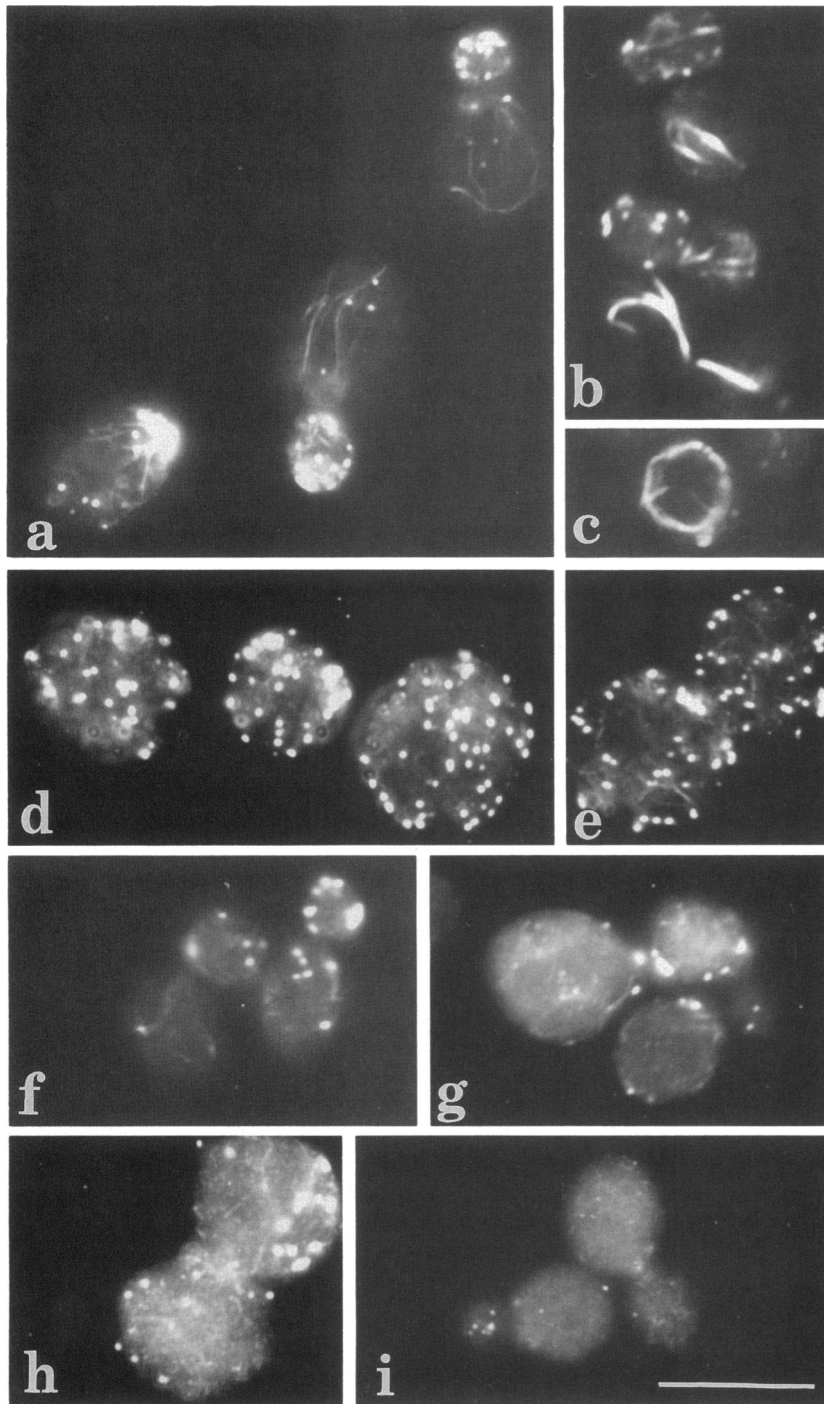
Figure 2. Anti-actin immunofluorescence of wild-type (a) and actin mutant (b–i) cells. Times indicate time after shift from 25 to 37°C. a, wild-type, 25°C; b, *act1-136/act1-136*, 25°C; c, *act1-132/act1-132*, 37°C, 90 min; d, *act1-101/act1-101*, 37°C, 45 min; e, *act1-101/act1-101*, 37°C, 45 min; f, *act1-129/act1-129*, 25°C; g, *act1-113/act1-113*, 25°C; h, *act1-113/act1-113*, 25°C; i, *act1-113/act1-113*, 37°C, 90 min. Bar, 10 μm.

act1-111, *act1-113*, and *act1-133* mutants reduced, but did not eliminate, the number of multibudded cells. In particular, a high proportion of the multibudded *act1-133* cells survived cell wall digestion.

The patterns of bud site selection in haploid and diploid *S. cerevisiae* cells are well characterized, and mutants that interfere with the axial (haploid) and/or bipolar (diploid) budding patterns and with bud growth have

been isolated. From studies on these various mutants, a model (reviewed by Drubin, 1991) for a genetic hierarchy emerged in which regulatory genes determine the site of bud emergence, and this information is then passed to the structural components that become assembled at the bud site. Actin and actin-binding proteins are among these structural components. Early in the cell cycle, patches containing filamentous actin and as-

Table 4. Fluorescence microscopy of wild-type and actin mutant cells

ACT1 Allele	Temp.[a] (°C)	Actin Organization[b] (immunofluorescence)	Nuclei	Mitochondrial Organization	Phalloidin Staining
WT/WT	25	Normal	Normal	Normal	Yes
WT/WT	37	Normal	Normal	Normal	ND
WT/Δ	25	Cables and patches present, reduced polarization of cortical patches, slightly fainter cables	1% binuc.	17% clumped	ND
WT/Δ	37	Patches delocalized, cables faint or missing	17.5% binuc.	25% clumped	ND
101/101	25	Chunks, some patch delocalization, short/faint cables	1.5% binuc.	17% clumped	Yes
101/101 (Fig. 2d, e)	37	Few or no cables, completely delocalized patches	4.1% binuc. (Fig. 3e, f)	50% clumped	ND
108/108	25	Some patch delocalization, elevated diffuse staining, 22% reduced staining of actin structures	2.8% binuc. (Fig. 3i, j)	25% clumped (Fig. 4g, h)	Yes
108/108	37	74% reduced staining of actin structures	9% binuc.	54% clumped	ND
111/111	25	50% delocalized patches, both patches and chunks often in bud and on mother cell side of bud neck, thin cables	15.9% multinuc.	Normal	Yes
111/111	37	84% delocalized patches, no cables	20.5% multinuc.	Normal	ND
113/113 (Fig. 2g, h)	25	Very high diffuse background, many cortical chunks, no cables visible, occasional cortical bars at either side of bud neck	3.5% multinuc. (Fig. 3g, h)	Normal	Yes
113/113 (Fig. 2i)	37	Very high diffuse background, fewer cortical chunks, more normal cortical patches, no cables visible	7.5% multinuc. (Fig. 3c, d)	Normal	ND
119/119	25	Normal except polarization of cortical patches to bud is reduced compared to wild type cells	3.0% binuc.	Normal	Yes
119/119	37	No cables, delocalized patches	24% binuc.	Mostly normal, some clumping	ND
120/120	25	High diffuse background, cables visible, delocalized cortical patches, variability with ∼25% having normal appearing actin staining	1.7% binuc.	12.5% clumped	Yes
120/120	37	No cables visible, higher diffuse background, delocalized patches	10% binuc.	19% clumped	ND
121/121	25	Patch delocalization, high diffuse background, 7.2% bars (94% bars associated with nucleus)[c]	1.9% binuc. 0.4% multinuc.	Normal	Yes
121/121	37	Patch delocalization, 0.9% bars (most bars associated with nucleus)	4.3% binuc.	2.8% clumped	ND
124/124	25	Some patch delocalization, chunks around bud neck, elevated diffuse staining	6.7% binuc. 2.5% multinuc.	Normal	Yes
124/124	37	Delocalized patches, no cables	12.6% binuc. 3.1% multinuc.	9.4% clumped	ND
125/125	25	10% normal actin staining, others have delocalized patches, elevated diffuse staining, faint cables	2.7% binuc.	6.2% clumped	Yes

Table 4. (Continued)

ACT1 Allele	Temp.[a] (°C)	Actin Organization[b] (immunofluorescence)	Nuclei	Mitochondrial Organization	Phalloidin Staining
125/125	37	Delocalized patches, elevated diffuse staining, faint cables, fewer cables than 25° cells	3.1% binuc.	18% clumped	ND
129/129 (Fig. 2f)	25	Cables present, but fewer than wild-type, chunks at either side of bud neck or elsewhere, often a few cables seem thicker than wild-type, punctate dots throughout cytoplasm	1% binuc.	Normal	No
129/129	37	Fewer chunks than at 25°C, delocalized patches, elevated diffuse background, fewer punctate cytoplasmic dots than at 25°C	ND	Normal	ND
132/132	25	Chunks and patches concentrated in bud, but less polarized than in wild type, 35.5% bars (72% bars associated with nucleus), elevated diffuse background	4.3% binuc. 1.7% multinuc.	6.8% clumped	Yes
132/132	37	Fewer chunks than at 25°C, delocalized patches, 25% bars (88% associated with nucleus)	8.9% binuc. 0.4% multinuc.	20% clumped (Fig. 4m, n)	ND
133/133	25	Elevated diffuse staining, delocalized patches, faint cables	ND	50% clumped (Fig. 4o, p)	Yes
133/133	37	Delocalized patches (apparently many more patches per surface area than wild-type), faint cables	10% multinuc.	90% clumped (Fig. 4i, j; k, l)	ND
136/136 (Fig. 2b)	25	High diffuse background, delocalized patches, chunks, punctate dots throughout cell, 32% have actin bars, 96% of which appear associated with the nucleus and 37% span only the length of the nucleus	6.3% binuc.	33% clumped	Yes
136/136	37	More chunks than at 25°C and more punctate dots throughout the cell, 17.9% have actin bars (the bars appear shorter than at 25°C), 97% of which appear associated with the nucleus	9.0% binuc.	57% clumped	ND

Clumped mitochondria: most or all of the mitochondria (as seen by DAPI staining) are so close to each other that single strands of mitochondria (mitochondrial DNA) of normal thickness can not be distinguished, and/or mitochondria are located in one area of the cell; *cortical actin chunks:* cortical patches that appear greater than twice the size of normal cortical actin patches. The chunks often appear to have irregular shapes.

[a] Cells were grown to early log phase and then were shifted to 37°C for 90 min.

[b] All percentages refer to the percentage of cells showing the phenotype. At least 200 cells were analyzed for all quantitation.

[c] In most cases the actin bars appeared to pass through the nucleus or to make a tangential interaction with the nuclear envelope. The nature of the interaction of the bars with the nucleus and whether they enter the nucleus or remain in the cytoplasm could not be determined by light microscopy.
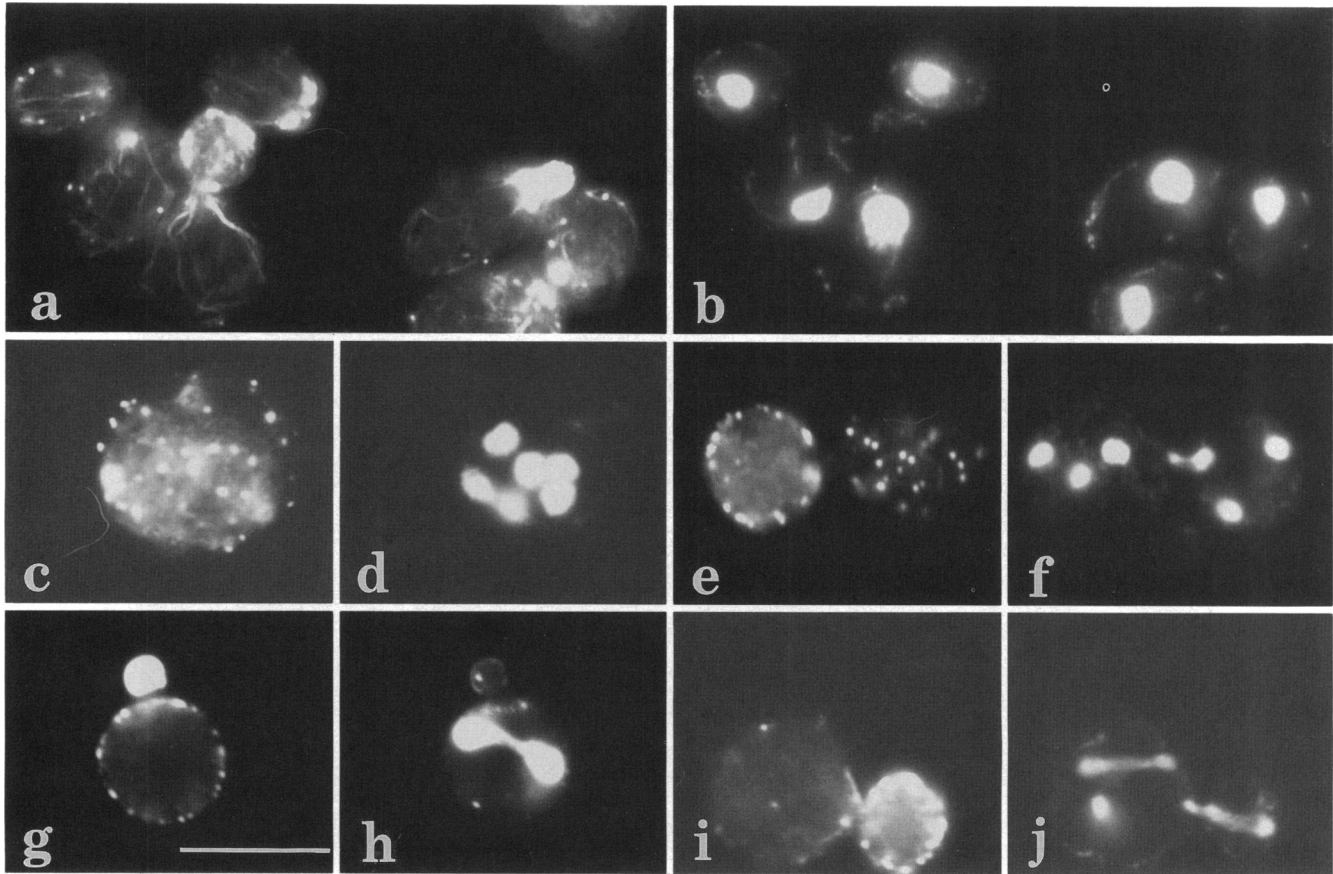
Figure 3. Anti-actin immunofluorescence (a, c, e, g, and i) and DAPI staining of nuclear DNA (b, d, f, h, and j), wild-type (a and b), and actin mutant (c–j) cells. The mutant alleles are as follows: c and d, *act1-113/act1-113*, 37°C, 90 min; e and f, *act1-101/act1-101*, 37°C, 45 min; g and h, *act1-119/act1-119*, 25°C; i and j, *act1-108/act1-108*, 25°C. Bar, 10 μm.

sociated proteins appear in a ring on the cortex of the unbudded cell (Adams and Pringle, 1984; Kilmartin and Adams, 1984). This ring marks the eventual position of the bud neck. An *ACT1/act1-Δ1::LEU2* hemizygote grown at 25°C is defective in bud site selection, showing an increase in random budding. In addition, the *act1-108*, *act1-113*, and *act1-124* alleles cause more severe defects in bud site selection at the permissive temperature than does the reduced *ACT1* gene dosage of the hemizygote. When analyzed for other phenotypes such as growth at different temperatures (Wertman *et al.*, 1992) and defects in cell morphology (Table 2), no other characteristics were identified that distinguished these three alleles from the other alleles. This includes defects in cytokinesis (Table 2). This latter point is of interest because Flescher *et al.* (1993) showed that mutations in *CDC10* and *SPA2* can cause defects in both bud site selection and cytokinesis. Although all *act1* alleles that severely affect bud site selection have cytokinetic defects, there are other alleles (e.g., *act1-133* and the *ACT1/act1-Δ1::LEU2* hemizygote) with marked cytokinetic defects (Table 2) that have only moderate effects on bud site selection (Table 3). Defects in the actin cyto-

skeleton might result in a failure to establish coordinates to be used for bud site selection in the subsequent cell cycle, or they might result in a failure to recognize such coordinates when forming a bud site, or both. Flescher *et al.* (1993) proposed that mutations that affect the ability to mark a bud site for the subsequent round of cell division will make a haploid cell have a bipolar budding pattern rather than an axial pattern, whereas a mutation that interferes with the targeting or assembly of proteins at the incipient bud site will lead to random budding patterns. By this model we would conclude that actin mutants are defective in the targeting and/or assembly of components at the incipient bud site. However, these issues cannot be definitively resolved until the molecular pathways of bud site selection and bud site assembly are elucidated.

Another phenotype that was not previously recognized for actin mutants is the appearance of aberrantly organized mitochondria. Although aberrant mitochondrial organization is observed in mutants defective in mitochondrial function (petites) (Pon and Schatz, 1991), the strains used in our studies showed, as is typical of diploid strains in general, very low rates
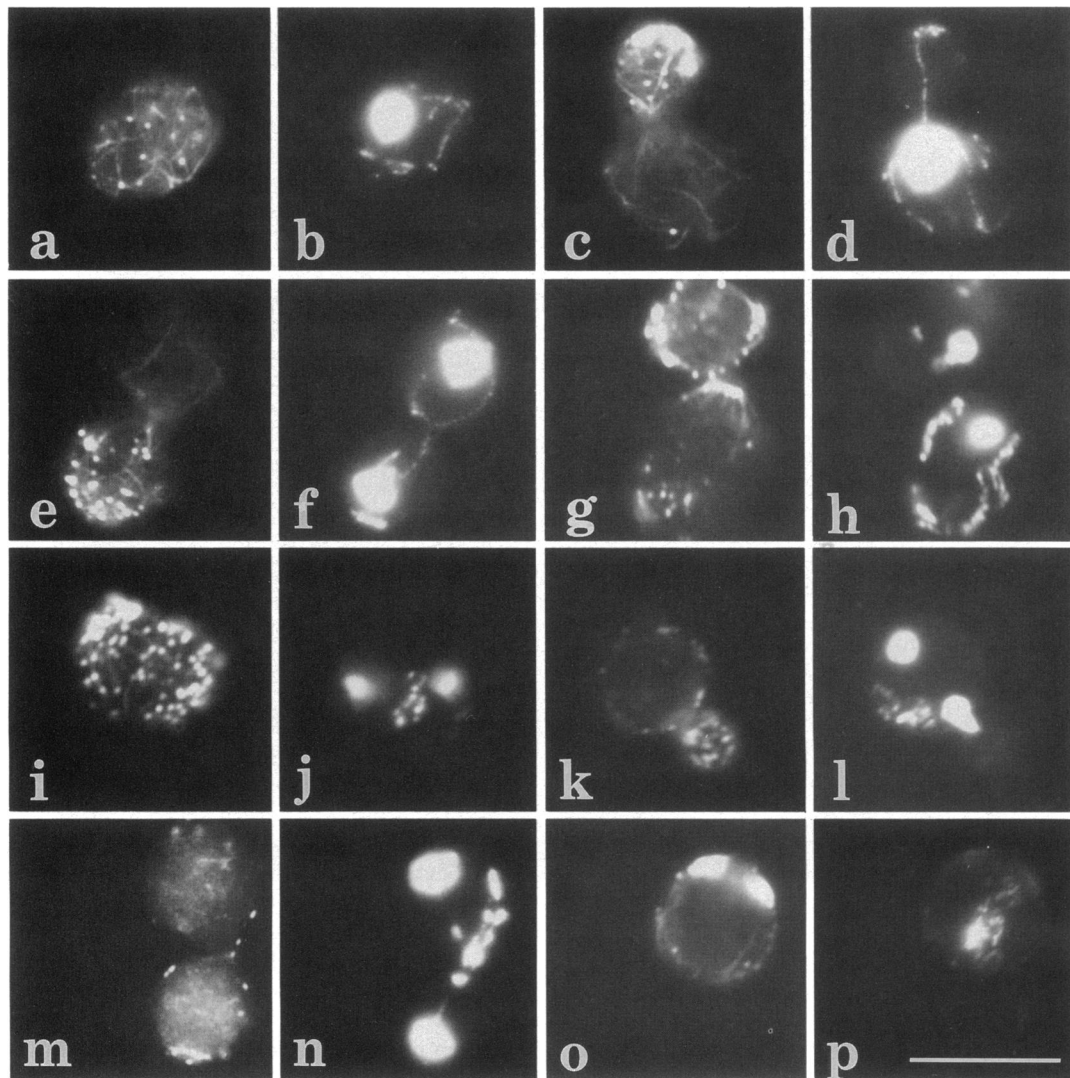
Figure 4. Anti-actin immunofluorescence (a, c, e, g, i, k, m, and o) and DAPI staining showing mitochondrial DNA (b, d, f, h, j, l, n, and p) in wild-type (a–f) and mutant (g–p) yeast. Mutant alleles are as follows: g and h, *act1-108/act1-108*, 25°C; i and j, *act1-133/act1-133*, 37°C, 90 min; k and l, *act1-133/act1-133*, 37°C, 90 min; m and n, *act1-132/act1-132*, 37°C, 90 min; o and p, *act1-133/act1-133*, 25°C. Bar, 10 μm.

(<1%) of petite formation. In further support of the possibility that actin-mitochondrial interactions are important for cytoplasmic organization of mitochondria, we found that at a high frequency ($\sim$20% of all cells examined) the mitochondrial strands of wild-type cells were colinear with actin cables. In the remaining cells, it is likely that the mitochondria were also associated with actin cables but that limitations in the ability to establish the spatial relationships of individual actin cables and mitochondrial DNA precluded identification of interactions. We conclude from the above observations that actin filaments play a role in organizing mitochondria in the cytoplasm.

The Phalloidin Binding Site on Actin

The atomic model of the actin filament (Holmes *et al.*, 1990) was generated by fitting the 2.8-Å structure of actin in a 1:1 complex with pancreatic DNase I (Kabsch *et al.*, 1990) to data on the filament structure derived from electron microscopy. This filament model provides a foundation for developing an understanding of the basis for actin-mediated processes at the level of molecular interactions in 3-D space. Refinement of the filament model requires tests independent of the methodology used to create the model. Our studies on phalloidin binding to mutant actins demonstrate the utility of the charged-to-alanine mutant actins for elucidating the interactions of specific actin residues and for refinement of the actin filament structure.

Phalloidin, a cyclic heptapeptide isolated from the mushroom *Amanita phalloides*, is a potent toxin that binds tightly to actin filaments and stabilizes them against disassembly (Wieland, 1977). Recently, Lorenz *et al.* (1993) applied a directed mutation algorithm to
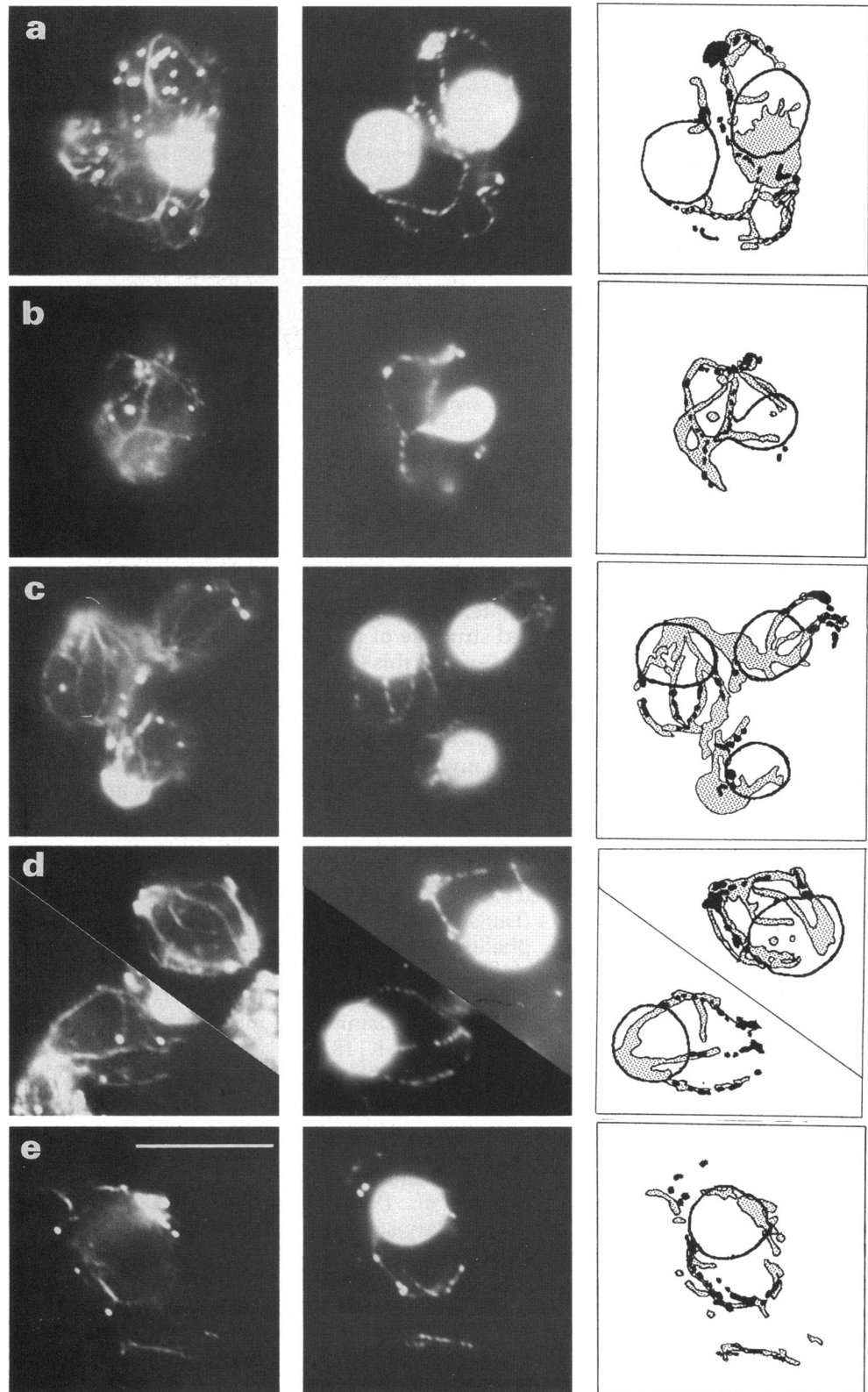
Figure 5. Anti-actin immunofluorescence (column one) and DAPI staining showing mitochondrial DNA (column two) of wild-type strain DDY440. Also shown (column three) are tracings, made by hand, of DAPI staining (black) and actin (stiples). Bar, 10 μm.
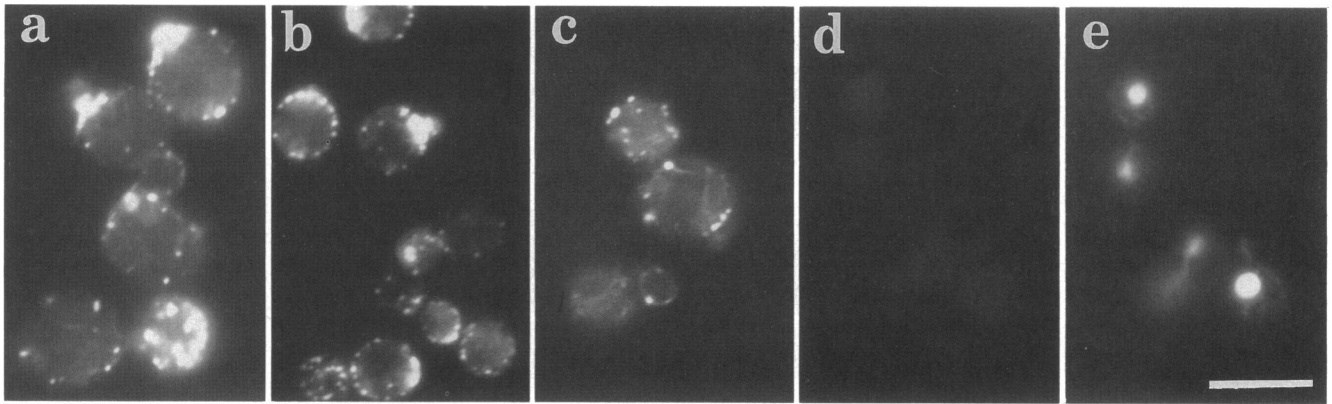
Figure 6. Anti-actin immunofluorescence (a and c) and rhodamine-phalloidin staining (b and d) of *act1-119/act1-119* (a and b) and *act1-129/act1-129* (c and d) mutants. Identical exposures were made for b and d. e shows DAPI staining of DNA for the same field of cells photographed in d. Bar, 10 μm.

X-ray fiber diffraction data collected from oriented gels of phalloidin-bound rabbit muscle actin filaments to refine the atomic model of the actin filament. A model for the phalloidin binding site on actin was generated. In this model, phalloidin binds in a cleft in the actin filament where it is in a position to interact with two or three monomers. The NMR-derived structure of phalloidin (Kessler and Wein, 1991) was used for this work. Figure 8 shows the molecular model for the position of phalloidin in the actin filament (coordinates kindly provided by Michael Lorenz, Max-Planck-Institute for Medical Research, Heidelberg, Germany). Three actin subunits are shown in yellow, red, and light purple.

Cross-linking studies, and now studies with actin mutants, have also been used as approaches to identify the phalloidin binding site on actin. Cross-linking studies implicated residues M119, E117, M355 (Vandekerckhove *et al.*, 1985), and C374 (Faulstich *et al.*, 1993) as potentially interacting with phalloidin. However, these residues, shown in white in Figure 8, are not proximal to the position of phalloidin derived from structural studies. Moreover, we find that rhodamine-phalloidin binds to *act1-119* (R116A, E117A, K118A) mutant actin filaments (see Figure 7) despite the fact that one of the residues that is altered in this mutant (E117) can be chemically cross-linked to phalloidin. Significantly, we find that rhodamine-phalloidin does not bind to *act1-129* (R177A, D179A; side chains colored green in Figure 8) (see also Wertman *et al.*, 1992 for localization of this mutation on a secondary structure drawing of the actin monomer) mutant actin. This effect is specific because defects in phalloidin binding were not observed for any other *act1* alleles and because *act1-129* does not cause particularly severe phenotypes compared to other *act1* alleles (Wertman *et al.*, 1992; this study). From these considerations, it is probable that one or both residues altered in *act1-129* interacts directly with phalloidin.

Our conclusion that residues R177 and/or D179 are important for phalloidin-binding is in good agreement

with the model for the phalloidin-binding site developed by Lorenz *et al.* (1993). For example in this model, the Oδ atom of residue D179 is 6 Å from the main chain of phalloidin (see Figure 8) (Lorenz *et al.*, 1993). However, whereas phalloidin and the implicated actin residues are in close proximity in the filament model, the distances between them are still too far for interactions such as hydrogen bonding. This is consistant with the fact that Lorenz *et al.* were not able to determine the orientation of phalloidin and shows here for the positioning of phalloidin and/or the implicated amino acid side chains in the filament model that molecular-genetic analyses can impose much needed constraints for the refinement of structural models.

Locating the binding site of phalloidin at a position where it can interact with two or three monomers in the actin filament provides a basis for understanding how this small cyclic peptide can stabilize an actin filament. In addition, although phalloidin binding does not typically block interactions of actin-binding proteins with actin (Miller and Alberts, 1989), it does inhibit the interaction of the filament-severing protein cofilin with actin filaments (Yonezawa *et al.*, 1988), and cofilin inhibits phalloidin binding to actin filaments (Nishida *et al.*, 1987), suggesting that cofilin might act to destabilize interactions in the filament at or near the region that phalloidin interacts with to stabilize filaments, focusing attention on this region as an important area for the control of filament stability.

Structure and Function of Yeast Actin

The atomic model of the actin filament provides a foundation for relating function, as determined by the phenotypes of actin mutants, to filament structure. The formation of abnormal actin bars that can be visualized by anti-actin immunofluorescence microscopy appears to result from a novel property imparted to actin by certain mutations. Thus, although some phenotypes observed for the charged-to-alanine point mutants also
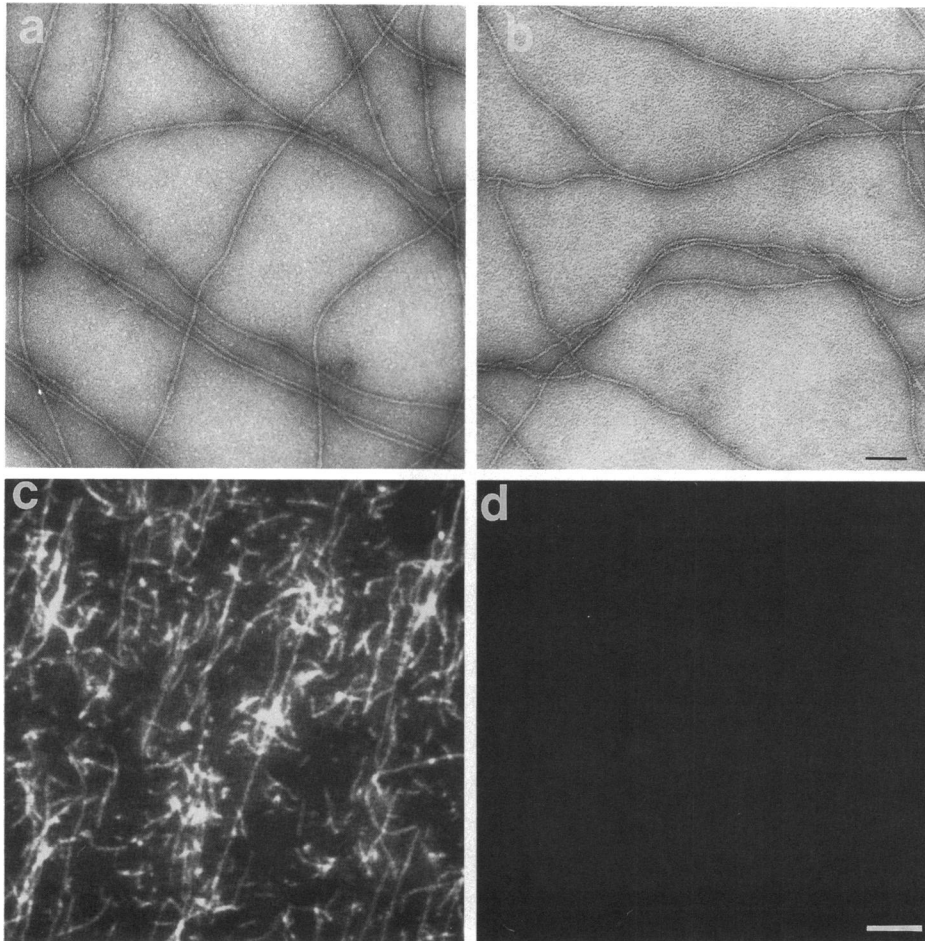
Figure 7. Electron microscopy (a and b) and rhodamine-phalloidin staining (c and d) of wild-type (a and c) and *act1-129* mutant (b and d) actin filaments. Actin filaments were visualized as described in MATERIALS AND METHODS. Bar in b for electron micrographs is 0.15 μm, bar in d for fluorescence micrographs is 3 μm.

appear in the *ACT1/act1-Δ1::LEU2* hemizygote (see Tables 2, 3, and 4), the hemizygous state does not lead to bar formation. Interestingly, the mutant alleles shown here to cause bar formation, *act1-121* (K83A, K84A), *act1-132* (R37A, R39A), *act1-136* (D2A), as well as *act1-2* (A58T), shown previously by Novick and Botstein (1985) to cause bar formation, all map to subdomains 1 and 2 on the outer surface of the actin filament. Whereas these bar structures are not likely to be physiologically important in wild-type yeast, the clustering of mutations that lead to bar formation on the outer surface of the filament implicates this surface in bar formation.

The observation mentioned above, that the *ACT1/act1-Δ1::LEU2* hemizygote shows a variety of phenotypes, raises an important consideration in interpreting our results in terms of the atomic structure model of actin. If a twofold decrease in actin levels can cause a variety of defects, then so might mutations that effect protein levels. This problem is especially problematic because changes in protein levels of less than twofold, which might effect actin functions, are hard to demonstrate. Thus, although we have not observed consistent effects of the charged-to-alanine mutations on actin

levels by immunoblotting, the limits of the sensitivity of this technique leave open the possibility that small changes in actin levels contribute to the mutant phenotype. With these caveats in mind, it is still likely that many mutations affect specific interactions of actin, just as the *act1-129* mutation specifically effects the interaction with phalloidin. First, the mutations are mostly near the surface of actin and are thus likely to only have local effects on actin structure, and they are in many different regions of the actin surface (Wertman *et al.*, 1992). Second, some phenotypes, e.g., the actin bar formation phenotype discussed above, are not observed for the *ACT1/act1-Δ1::LEU2* hemizygote. Finally, the mutants show different constellations of phenotypes (this study) and genetic properties (Wertman *et al.*, 1992) rather than a monotonic progression of increasing phenotypic severity.

A number of the charged-to-alanine mutations studied here fall under the "myosin footprint" (Rayment *et al.*, 1993; Schroder *et al.*, 1993) and therefore provide opportunities to test the importance of the implicated residues for interactions with myosin and for cell physiology. Three alleles, *act1-120* (E99A, E100A), *act1-133* (D24A, D25A), and *act1-136* (D2A), have alterations in
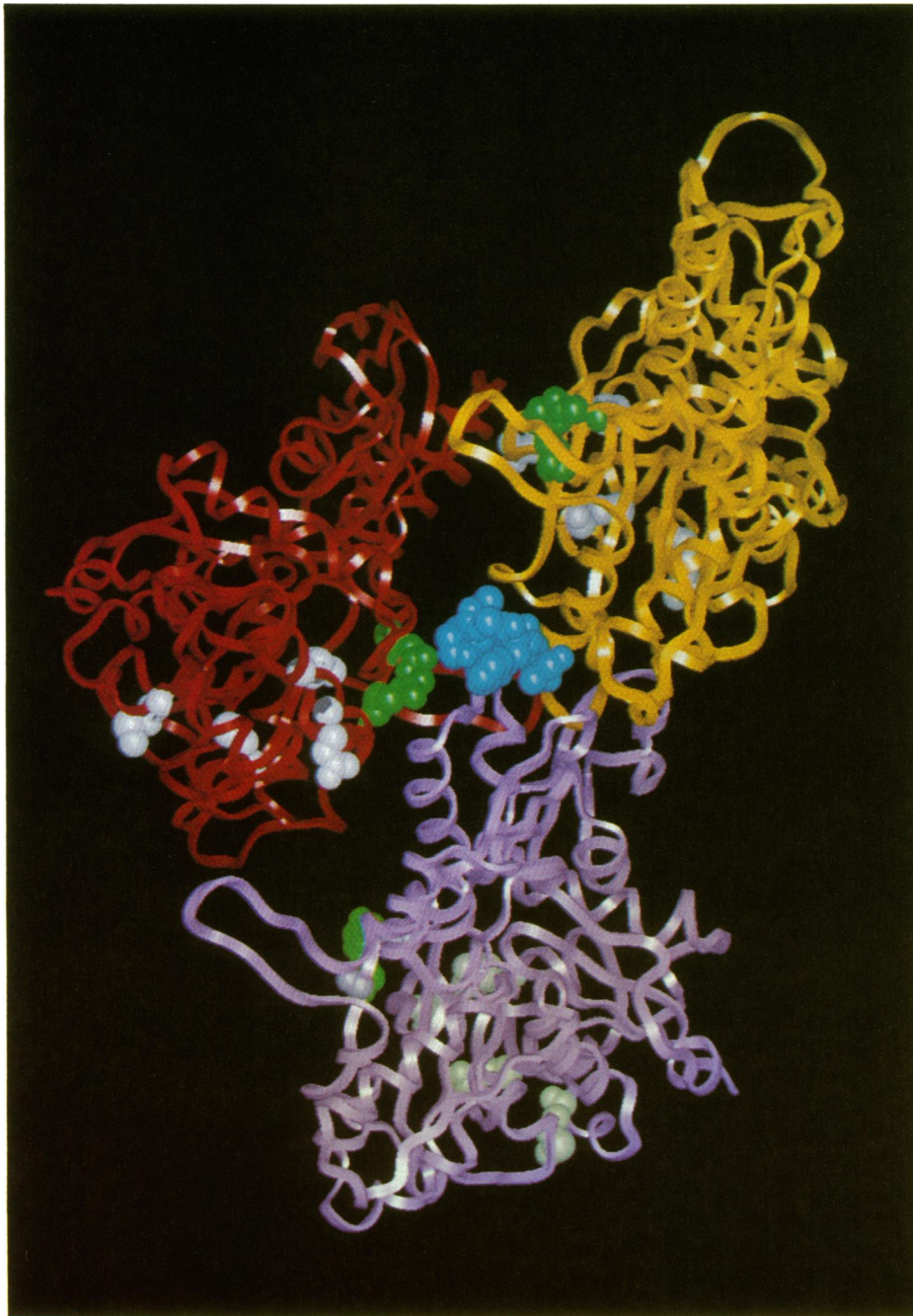
Figure 8. Molecular graphics showing Lorenz *et al.* (1993) model of an actin trimer (yellow, red, light purple) with bound phalloidin (blue). Side chains of residues changed in the *act1-129* mutant allele (R177A, D179A) that fails to bind rhodamine phalloidin are shown in green. The side chains of various residues (117, 119, 355, 374) that have been chemically cross-linked to phalloidin (Vandekerckhove *et al.*, 1985; Faulstich *et al.*, 1993) are shown in white. In the *act1-119* (R116A, E117A, K118A) mutant allele one of the residues (E117) that has been cross-linked to phalloidin is changed to alanine without a noticable affect on phalloidin binding.

residues proposed to make electrostatic interactions with a lysine-rich loop of myosin (rabbit muscle myosin residues 626–647) (Schroder *et al.*, 1993). Indeed, filaments assembled from mutant *Dictyostelium* actins D24H/ D25H and E99H/E100H are defective in ATP-driven sliding on myosin-coated surfaces (Johara *et al.*, 1993). In addition, the residues altered in *act1-101* (D363A, E364A) are suggested to interact with myosin alkaline light chain I (Sutoh, 1982; Trayer *et al.*, 1987), and the residues altered in *act1-132* (R37A, R39A) are proximal

to a contact region consisting of H40 through G42 (Rayment *et al.*, 1993).

Of the mutants with amino acid substitutions under or near the myosin footprint, all have defects in mitochondrial organization. The two alleles that cause the most dramatic mitochondrial defects, *act1-133* and *act1-136*, alter residues implicated in the interaction with the lysine-rich loop of myosin, as does *act1-120*, which has a less severe, but significant, mitochondrial defect. Other alleles with alterations in or near the

myosin footprint *act1-101* and *act1-132* are also defective in mitochondrial organization. Two alleles, *act1-108* (R256A, E259A) and *act1-125* (K50A, D51A), with dramatic and mild effects on mitochondrial organization, respectively, alter residues that should not interact directly with myosin based on the present actin-myosin interaction model. These mutations might have indirect effects on actin-myosin interactions, perhaps by causing conformational changes in actin or by altering the interaction with tropomyosin, or they might effect other interactions that are important for mitochondrial organization.

The above observations suggest that actin-myosin interactions might underlie the cytoplasmic organization of mitochondria. If this is true, we would predict that other yeast actin mutants altered in myosin interactions (Cook *et al.*, 1992, 1993) would show altered mitochondrial organization, and that mutations in one or more of the yeast myosin genes would also create a similar phenotype. We note that *act1-133* mutants, in addition to having mitochondrial defects, grow large and multinucleate, a phenotype that has been seen for *myo2* (Johnston *et al.*, 1991) and *tpm1* (Liu and Bretscher, 1992) mutants. It is possible that different *act1* alleles affect interactions with different myosins differentially, and/or that the cell has different thresholds for the reduction of interactions of actin with different myosins. These factors could determine the phenotypes associated with distinct mutations in residues under the myosin footprint. Thus hypothetically, the *act1-133* mutation might have an especially detrimental affect on the interaction with the Myo2 myosin. Biochemical assays (Kron *et al.*, 1992) to determine how different *act1* alleles affect interactions with different yeast myosins might help to elucidate the in vivo roles of the different yeast myosins.

In summary, the recent reports of atomic models of actin (Kabsch *et al.*, 1990) and actin filaments alone (Holmes *et al.*, 1990) and in complexes with phalloidin (Lorenz *et al.*, 1993), and fragments of myosin (Rayment *et al.*, 1993; Schroder *et al.*, 1993) and gelsolin (McLaughlin *et al.*, 1993), provide opportunities to develop a deep mechanistic understanding of how actin interacts with a variety of proteins and ligands to control many aspects of a cell's biology. The synthesis of information from biochemical, structural, genetic, and molecular-genetic studies is required to attain this goal. In this study, analysis of a collection of charged-to-alanine mutants, expressed as the only source of actin in vivo, proved valuable for associating specific regions of actin with roles in mitochondrial organization and phalloidin binding.

ACKNOWLEDGMENTS

REFERENCES

Adams, A.E., Johnson, D.I., Longnecker, R.M., Sloat, B.F., and Pringle, J.R. (1990). CDC42 and CDC43, two additional genes involved in budding and the establishment of cell polarity in the yeast *Saccharomyces cerevisiae*. J. Cell Biol. *111*, 131–142.

Adams, A.E.M., and Pringle, J.R. (1984). Relationship of actin and tubulin distribution in wild-type and morphogenetic mutant *Saccharomyces cerevisiae*. J. Cell Biol. *98*, 934–945.

Bass, S.H., Mulkerrin, M.G., and Wells, J.A. (1991). A systematic mutational analysis of hormone-binding determinants in the human growth hormone receptor. Proc. Natl. Acad. Sci. USA *88*, 4498–4502.

Bender, A., and Pringle, J.R. (1991). Use of a screen for synthetic-lethal and multicopy-suppressee mutants to identify two new genes involved in morphogenesis in *Saccharomyces cerevisiae*. Mol. Cell. Biol. *11*, 1295–1305.

Bennett, W.F., Paoni, N.F., Keyt, B.A., Botstein, D., Jones, A.J., Presta, L., Wurm, F.M., and Zoller, M.J. (1991). High resolution analysis of functional determinants on human tissue-type plasminogen activator. J. Biol. Chem. *266*, 5191–5201.

Chant, J., and Herskowitz, I. (1991). Genetic control of bud site selection in yeast by a set of gene products that constitute a morphogenetic pathway. Cell *65*, 1203–1212.

Chowdhury, S., Smith, K.W., and Gustin, M.C. (1992). Osmotic stress and the yeast cytoskeleton: phenotype-specific suppression of an actin mutation. J. Cell Biol. *118*, 561–571.

Cook, R.K., Blake, W.T., and Rubenstein, P.A. (1992). Removal of the amino-terminal acidic residues of yeast actin. Studies in vitro and in vivo [published erratum appears in J. Biol. Chem. 1992 Jul 5; 267, 13780]. J. Biol. Chem. *267*, 9430–9436.

Cook, R.K., Root, D., Miller, C., Reisler, E., and Rubenstein, P.A. (1993). Enhanced stimulation of myosin subfragment 1 ATPase activity by addition of negatively charged residues to the yeast actin NH2 terminus. J. Biol. Chem. *268*, 2410–2415.

Drubin, D.G. (1991). Development of cell polarity in budding yeast. Cell *65*, 1093–1096.

Drubin, D.G., Miller, K.G., and Botstein, D. (1988). Yeast actin-binding proteins: evidence for a role in morphogenesis. J. Cell Biol. *107*, 2551–2561.

Dunn, T.M., and Shortle, D. (1990). Null alleles of SAC7 suppress temperature-sensitive actin mutations in *Saccharomyces cerevisiae*. Mol. Cell. Biol. *10*, 2308–2314.

Faulstich, H., Zobeley, S., Heintz, D., and Drewes, G. (1993). Probing the phalloidin binding site of actin. FEBS Letts. *318*, 218–222.

Flescher, E.G., Madden, K., and Snyder, M. (1993). Components required for cytokinesis are important for bud site selection in yeast. J. Cell Biol. *122*, 373–386.

Ford, S.K., and Pringle, J.R. (1991). Cellular morphogenesis in the *Saccharomyces cerevisiae* cell cycle: localization of the CDC11 gene product and the timing of events at the budding site. Dev. Genet. *12*, 281–92.

Gallwitz, D., and Seidel, R. (1980). Molecular cloning of the actin gene from yeast *Saccharomyces cerevisiae*. *Nucleic Acids Res. 8*, 1043–1059.

Gibbs, C.S., and Zoller, M.J. (1991). Rational scanning mutagenesis of a protein kinase identifies functional regions involved in catalysis and substrate interactions. J. Biol. Chem. *266*, 8923–8931.

Greer, C., and Schekman, R. (1982). Actin from *Saccharomyces cerevisiae*. Mol. Cell. Biol. *2*, 1270–1278.

Holmes, K.C., Popp, D., Gebhard, W., and Kabsch, W. (1990). Atomic model of the actin filament. Nature *347*, 44–49.

Holtzman, D.A., Yang, S., and Drubin, D.G. (1993). Synthetic-lethal interactions identify two novel genes, SLA1 and SLA2, that control membrane cytoskeleton assembly in *Saccharomyces cerevisiae*. J. Cell Biol. *122*, 635–644.

Johannes, F.J., and Gallwitz, D. (1991). Site-directed mutagenesis of the yeast actin gene: a test for actin function in vivo. EMBO J. *10*, 3951–3958.

Johara, M., Toyoshima, Y.Y., Ishijima, A., Kojima, H., Yanagida, T., and Sutoh, K. (1993). Charge-reversion mutagenesis of *Dictyostelium* actin to map the surface recognized by myosin during ATP-driven sliding motion. Proc. Natl. Acad. Sci. USA *90*, 2127–2131.

Johnston, G.C., Prendergast, J.A., and Singer, R.A. (1991). The *Saccharomyces cerevisiae* MYO2 gene encodes an essential myosin for vectorial transport of vesicles. J. Cell Biol. *113*, 539–551.

Kabsch, W., Mannherz, H.G., Suck, D., Pai, E.F., and Holmes, K.C. (1990). Atomic structure of the actin: DNase I complex. Nature *347*, 37–44.

Kessler, H., and Wein, T. (1991). Solution structure of phalloidin obtained by NMR spectroscopy in [D6]DMSO and molecular dynamics calculation in vacuo and in water. Liebigs Annalen der Chemie *2*, 179–184.

Kilmartin, J., and Adams, A.E.M. (1984). Structural rearrangements of tubulin and actin during the cell cycle of the yeast *Saccharomyces*. J. Cell Biol. *98*, 922–933.

Kron, S.J., Drubin, D.G., Botstein, D., and Spudich, J.A. (1992). Yeast actin filaments display ATP-dependent sliding movement over surfaces coated with rabbit muscle myosin. Proc. Natl. Acad. Sci. USA *89*, 4466–4470.

Kubler, E., and Riezman, H. (1993). Actin and fimbrin are required for the internalization step of endocytosis in yeast. EMBO J. *12*, 2855–2862.

Liu, H., and Bretscher, A. (1992). Characterization of TPM1 disrupted yeast cells indicates an involvement of tropomyosin in directed vesicular transport. J. Cell Biol. *118*, 285–299.

Lorenz, M., Popp, D., and Holmes, K.C. (1993). Refinement of the F-actin model against X-ray fiber diffraction data by the use of a directed mutation algorithm. J. Mol. Biol. *234*, 826–836.

McLaughlin, P.J., Gooch, J.T., Mannherz, H.-G., and Weeds, A.G. (1993). Structure of gelsolin segment 1-actin complex and the mechanism of filament severing. Nature *364*, 685–692.

Miller, K.G., and Alberts, B.M. (1989). F-actin affinity chromatography: technique for isolating previously unidentified actin-binding proteins. Proc. Natl. Acad. Sci. USA *86*, 4808–4812.

Millonig, R., Salvo, H., and Aebi, U. (1988). Probing actin polymerization by intermolecular cross-linking. J. Cell Biol. *106*, 785–796.

Nefsky, B., and Bretscher, A. (1992). Yeast actin is relatively well behaved. Eur. J. Biochem. *206*, 949–955.

Ng, R., and Abelson, J. (1980). Isolation of the gene for actin in *Saccharomyces cerevisiae*. Proc. Natl. Acad. Sci. USA *77*, 3912–3916.

Nishida, E., Iida, K., Yonezawa, N., Koyasu, S., Yahara, I., and Sakai, H. (1987). Cofilin is a component of intranuclear and cytoplasmic actin rods induced in cultured cells. Proc. Natl. Acad. Sci. USA *84*, 5262–5266.

Novick, P., and Botstein, D. (1985). Phenotypic analysis of temperature-sensitive yeast actin mutants. Cell *40*, 405–416.

Palmer, R.E., Sullivan, D.S., Huffaker, T., and Koshland, D. (1992). Role of astral microtubules and actin in spindle orientation and migration in the budding yeast, *Saccharomyces cerevisiae*. J. Cell Biol. *119*, 583–593.

Pon, L., and Schatz, G. (1991). Biogenesis of yeast mitochondria. In: The Molecular Biology of the Yeast *Saccharomyces:* Genome Dynamics, Protein Synthesis and Energetics, vol. 1, ed. J.R. Broach, J.R. Pringle, and E.W. Jones, Cold Spring Harbor, NY: Cold Spring Harbor Press, 333–406.

Pringle, J.R., Preston, R.A., Adams, A.E., Stearns, T., Drubin, D.G., Haarer, B.K., and Jones, E.W. (1989). Fluorescence microscopy methods for yeast. Methods Cell Biol. *31*, 357–435.

Rayment, I., Holden, H.M., Whittaker, M., Yohn, C.B., Lorenz, M., Holmes, K.C., and Milligan, R.A. (1993). Structure of the actin-myosin complex and its implications for muscle contraction. Science *261*, 58–65.

Read, E.B., Okamura, H.H., and Drubin, D.G. (1992). Actin- and tubulin-dependent functions during *Saccharomyces cerevisiae* mating projection formation. Mol. Biol. Cell *3*, 429–444.

Schroder, R.R., Manstein, D.J., Jahn, W., Holden, H., Rayment, I., Holmes, K.C., and Spudich, J.A. (1993). Three-dimensional atomic model of F-actin decorated with *Dictyostelium* myosin S1. Nature *364*, 171–174.

Schulze, E., and Kirschner, M.W. (1986). Microtubule dynamics in interphase cells. J. Cell Biol. *102*, 1020–1031.

Shortle, D., Novick, P., and Botstein, D. (1984). Construction and genetic characterization of temperature-sensitive mutant alleles of the yeast actin gene. Proc. Natl. Acad. Sci. USA *81*, 4889–4893.

Sutoh, K. (1982). Identification of myosin-binding sites on the actin sequence. Biochemistry *21*, 3654–3661.

Trayer, I.P., Trayer, H.R., and Levine, B.A. (1987). Evidence that the N-terminal region of A1-light chain of myosin interacts directly with the C-terminal region of actin. A proton magnetic resonance study. Eur. J. Biochem. *164*, 259–66.

Vandekerckhove, J., Deboben, A., Nassal, M., and Wieland, T. (1985). The phalloidin binding site of F-actin. EMBO J. *4*, 2815–2818.

Watts, F.Z., Shiels, G., and Orr, E. (1987). The yeast MYO1 gene encoding a myosin-like protein required for cell division. EMBO J. *6*, 3499–3505.

Wertman, K.F., and Drubin, D.G. (1992). Actin constitution: guaranteeing the right to assemble. Science *258*, 759–760.

Wertman, K.F., Drubin, D.G., and Botstein, D. (1992). Systematic mutational analysis of the yeast *ACT1* gene. Genetics *132*, 337–350.

Wieland, T. (1977). Modification of actins by phallotoxins. Naturwissenschaften *64*, 303–309.

Yonezawa, N., Nishida, E., Maekawa, S., and Sakai, H. (1988). Studies on the interaction between actin and cofilin purified by a new method. Biochem. J. *251*, 121–127.